Available online at www.sciencedirect.com

ScienceDirect

journal homepage: www.elsevier.com/locate/issn/15375110

Research Paper

Online detection of naturally DON contaminated wheat grains from China using Vis-NIR spectroscopy and computer vision

Xueming He [a,b], *Tianxia Zhao* [a,b], *Fei Shen* [a,b,*], *Qin Liu* [a,b], *Yong Fang* [a,b], *Qiuhui Hu* [a,b]

[a] College of Food Science and Engineering, Nanjing University of Finance and Economics, Nanjing 210023, China
[b] Collaborative Innovation Center for Modern Grain Circulation and Safety, Nanjing 210023, China

ARTICLE INFO

Article history:
Received 20 June 2020
Received in revised form
26 October 2020
Accepted 11 November 2020
Published online 26 November 2020

Keywords:
Vis-NIR spectroscopy
Computer vision
Wheat grains
DON
Features fusion

Deoxynivalenol (DON) contamination of wheat grains is a serious problem in China, and it is necessary to remove contaminated wheat before it enters the consumer market. In this study, visible-near infrared (Vis-NIR) spectroscopy and computer vision techniques were combined to simulate online discrimination between normal and DON-contaminated wheat grains. Naturally growing wheat samples were collected from several of the main wheat-producing areas in China, the reference DON contents were measured by using liquid chromatography serial triple quadrupole mass spectrometer (LC-MS), and then wheat samples were divided into two categories according to the national standard of 1 mg kg^{-1}. The characteristic spectral variables, colour and texture features were extracted and integrated for chemometric analysis. Principal component analysis based on fusion features indicated better clustering than with just spectral features. Subsequently, linear discriminant analysis modelling based on spectra and texture features achieved the best discrimination with an accuracy of 95.06% and 91.36% for calibration and validation sets respectively, which was 5% higher than with just spectral features, and the false positive rates (*FPR*) were the lowest: 3.41% and 10.42% for calibration and validation sets respectively. The internal scanning results of whole wheat flour indicated that the higher the content of DON, the looser the binding of starch granules, which could cause the textural change of wheat grains. The research showed that Vis-NIR spectroscopy combined with computer vision has the potential to be used in the non-destructive and online detection of DON-contaminated wheat grains; further study on the interference from complex environments is still need for actual online detection.

* *Corresponding author*. College of Food Science and Engineering, Nanjing University of Finance and Economics, Nanjing 210023, China.
E-mail address: shenfei@nufe.edu.cn (F. Shen).

https://doi.org/10.1016/j.biosystemseng.2020.11.001
1537-5110/

Nomenclature

ASM	Angular second moment
CARS	Competitive adaptive reweighted sampling
CCD	Charge coupled device
CCR	Correct classification rate (%)
CON	Contrast
COR	Correlation
DON	Deoxynivalenol
ELISA	Enzyme-linked immunosorbent assay
ENT	Entropy
FPR	False positive rate (%)
FNR	False negative rate (%)
GC	Gas chromatography
HPLC	High performance liquid chromatography
KS	Kennard-Stone
LC-MS	Liquid chromatography serial triple quadrupole mass spectrometer
LDA	Linear discriminant analysis
PC	Principal component
PLS-DA	Partial least squares discrimination analysis
PLSR	Partial least squares regression
RGB	Red, green, blue
SD	Standard deviations
SNV	Standard normal variate transformation
SVM	Support vector machine
SPA	Successive projection algorithm
TLC	Thin-layer chromatography
Vis-NIR	Visible-near infrared

1. Introduction

Wheat grains are rich in starch, protein, lipids, minerals and other nutrients, and can be used in the development of highly nutritious and functional food. However, they have no shell protection, thin cortex, soft structure, a lot of hydrophilic substances and strong moisture absorption capacity. Compared with maize and rice, wheat is more prone to breeding pests and mould. *Fusarium* head blight is a worldwide wheat disease, which brings a great loss to wheat production worldwide every year (Bai & Shaner, 2004). In addition to causing yield loss, mycotoxins such as deoxynivalenol (DON) can be produced in the process of *F. graminearum* infection, and this can seriously affect the quality and commodity value of wheat, and poison people and animals (Walter et al., 2010). Therefore, it is necessary to be able to estimate the DON levels in wheat grains before they enter the food chain.

At present, there are several commonly used methods for identifying DON contents, including thin-layer chromatography (TLC, Rocha et al., 2017), high performance liquid chromatography (HPLC, Moazami & Jinap, 2009), enzyme-linked immunosorbent assay (ELISA, Li et al., 2012), Gas chromatography (GC, Cunha & Fernandes, 2012). All of these methods require trained operators and the use of unfriendly chemicals, are destructive in nature, take a long time for the examination of a single sample, and have high cost, which limits their feasibility for real time measurements. Therefore, an effective, rapid and non-destructive method is needed for wheat safety control.

Spectroscopic and imaging-based sensing techniques are increasingly being studied as potential alternatives to chemical approaches, for their advantages of little or no sample pretreatment, high accuracy, fast and non-invasive detection with robust and cost-efficient sensor technology available nowadays (He et al., 2018). Among them, visible and near infrared (Vis-NIR) spectroscopy and computer vision techniques have great potential in the online detection of foodstuffs and have been widely used in practice (Qu et al., 2015). Because metabolic activity of toxigenic fungus in samples can result in considerable change in the chemical parameters and physical characteristics, so these two techniques could be promising tools for non-destructive detection of contaminated foodstuffs (Wu et al., 2018). In recent years, many scholars have applied NIR spectroscopy to the rapid analysis of mycotoxin contamination in grains (Hossain & Goto, 2014). De Girolamo et al. (2019) analysed the ochratoxin A contaminated wheat grains using Fourier transform NIR and Fourier transform mid-infrared spectroscopy. The threshold of ochratoxin A was set to 2 $\mu g\ kg^{-1}$, and the results showed that both discrimination accuracies are higher than 94%. Shen et al. (2018) applied NIR and electronic nose techniques to the detection of *Aspergillus* spp. contamination levels in peanuts (acceptable: colony counts log CFU/g < 2.7, mouldy: log CFU/g ≥ 2.7), and the linear discriminant analysis (LDA) results showed correct classification rates of 92.11% and 86.84% respectively. Dvoáek et al. (2012) quantitatively predicted the DON contents of wheat grains by using NIR spectroscopy, and a correlation coefficient of 0.88 was obtained by partial least squares regression (PLSR). As for computer vision, Bayraktar et al. (2006) demonstrated an application of computer vision and pattern-recognition techniques to classify scatter patterns formed by *Listeria* colonies. Wang et al. (2014) developed a selective growth medium and a more rapid detection method based on computer vision for selective isolation and identification of *Staphylococcus aureus* in foods. Both studies suggested the feasibility of image-based bio-detection systems. There have been a number of reports of the detection of mildewed nuts based on colour (Chen et al., 2011; Kumar et al., 2010) and texture (Chen et al., 2007) information. However, there have been few reports that applied computer vision to the detection of mycotoxins in grains. In general, most studies have been conducted under laboratory conditions and have focused on static detection, so feasibility studies of online detection of DON contents in wheat grains are urgently needed.

In this study, naturally-grown wheat grain samples (normal and diseased) have been collected from several of the main-producing areas in China and were assessed with no inoculation and with simulated storage. The Vis-NIR and computer vision techniques were combined to realise online discrimination of normal and DON contaminated wheat grains, and the specific components of this study were: (1) to build a dynamic detection system for simulating online detection to obtain the spectral and image information; (2) to collect and extract the optimal spectral and image features of wheat grain samples; (3) to integrate spectral and image features for discrimination of different DON levels in wheat

grains; (4) to compare the results of different feature integrations and analyse the effects.

2. Materials and methods

2.1. Sample preparation and DON content measurement

The wheat grain samples used in this study were provided by Shandong CDC, Jiangsu Provincial Food and Strategic Reserves Administration. A total of 243 samples were tested in this study, coming from 6 main producing areas in China in 2018 and 2019, with different varieties. Each sample was collected from different fields, and the total size for each sample was about 5 kg. Considering DON level varies from one kernel to another, the wheat kernels in each sample were mixed adequately. Table 1 shows the specific information for all samples. They were all refrigerated at −4 °C before analysis.

DON contents of wheat grains were measured by liquid chromatography serial triple quadrupole mass spectrometer (LC-MS/MS, Waters-UPLC Xevo TQ, Waters, USA). Following methods in the published literature (Pasquali et al., 2019), about 400 g wheat grain were firstly ground by milling machine (Tube Mill 100 control, IKA, Germany) to obtain wheat flour. A sample of 2.5 g of wheat flour was weighed and placed in a 50 mL centrifuge tube, then 10 mL of 1% acetic acid-water solution was added to the tube, vortexed and placed in a refrigerator at 4 °C for 10 min. Then 10 mL of acetonitrile was added and vortexed for 2 min, then a salt packet (4 g of magnesium sulfate and 1 g of sodium acetate) was added, vortexed again for 2 min, and centrifuged at 6000 r min^{-1} for 5 min at 4 °C. A sample of 1 mL of the supernatant, after passing through a 0.22 μm organic filter, was taken to test.

Chromatographic conditions: Liquid phase system: Waters ACQUITY UPLC H-class; column: ACQUITY UPLC BEHC18 (1.7 μm, 2.1 mm × 100 mm); column temperature: 40 °C; detection period: 6 min; injection volume: 10 μL; mobile phase: A (0.1% formic acid-water), B (acetonitrile). The gradient elution conditions are given in Table 2.

Mass spectrometry conditions: Mass spectrometry system: Xevo TQ MS; ionisation mode: ESI+; capillary voltage: 3 KV; desolvation temperature: 500 °C; desolvation flow rate: 1000 L h^{-1}; set retention time 1.36 s, monitoring ion pair 297.1 > 231.1 (quantitative ion pair, cone hole voltage 25 V, collision energy 13 V, dwell time 0.052 s) and 297.1 > 249.1 (cone hole voltage 25 V, collision energy 10 V, dwell time 0.052 s).

The linear range of detection of DON for LC-MS/MS is 0.040–8.00 mg kg^{-1}, and the detection limit is 4.664 μg kg^{-1}. Fortified recovery rates were also calculated and they all ranged from 70.40% to 81.10%. Samples were determined with triplicate measurements and relative standard deviation (% RSD) was between 2.53% and 8.09%.

After the LC-MS measurement, all wheat samples were divided into two categories (normal: ≤ 1 mg kg^{-1}, DON contaminated: > 1 mg kg^{-1}) according to a threshold of 1 mg kg^{-1}, which is China-regulated limit in foods and feeds (GB2761-2017).

Table 1 – Summary table of wheat sample information at different sampling locations.

Sampling location	Number	Range of DON (mg kg^{-1})	Mean of DON (mg kg^{-1})	Standard deviation of DON (mg kg^{-1})
Jinan city	111	0–3.070	0.395	0.490
Shijiazhuang city	10	0.627–0.949	0.767	0.105
Zhengzhou city	29	0.443–4.211	1.454	0.977
Huai'an city	68	0.010–7.200	2.389	1.149
Yancheng city	19	1.230–5.591	2.986	1.205
Yangzhou city	6	1.131–3.206	1.915	0.743
Sum	243	0–7.200	1.335	1.288

Table 2 – Mobile phase gradient elution procedures.

Time (min)	Flow rate (mL min^{-1})	A (%)	B (%)
0	0.4	90	10
0.2	0.4	90	10
3.0	0.4	40	60
3.5	0.4	10	90
4.5	0.4	10	90
4.6	0.4	90	10
6.0	0.4	90	10

2.2. Instrumentation and data acquisition

As shown in Fig. 1, the dynamic detection system developed in this study mainly consists of four parts: Vis-NIR spectroscopy section, computer vision section, conveyor belt section and computer. In Vis-NIR spectroscopy section, a Zeiss MCS 600 spectrometer series (Carl Zeiss, Oberkochen, Germany) was used to collect the spectra of samples, which included two fibre spectrometers (MCS 611 VI: 380–1050 nm; MCS 611 NIR 1.7: 950–1690 nm). The two spectrometers were connected with a diffuse reflection probe by a Y-type optical fibre, and the probe internally equipped with a 5 V, 10 W halogen lamp. The distance between the upper surface of wheat grains and the probe was 2.0 cm. In the computer vision section, a charge coupled device (CCD) camera (Microvision, Shanxi, China) was

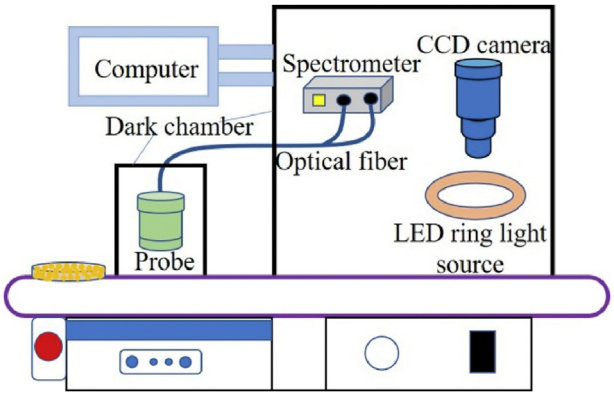

Fig. 1 – Schematic diagram of dynamic detection system.

placed at the top of dark box for image capture, and a LED ring light source (18 W, Microvision, Shanxi, China) was fixed under the camera. The distance between the camera and LED was 15 cm, which should ensure that the light irradiates the sample evenly without causing any ghost interference.

In spectral and imaging analysis, about 400 g subsample was randomly taken from the total sample size. During each acquisition, about 20 g wheat kernels were taken and placed on the conveyor belt in a non-reflective and shallow tray (diameter = 9 cm, height = 1.5 cm), and the speed of the belt was adjusted to a maximum of 0.15 m s^{-1}. Diffuse reflectance spectra of wheat grains were collected using Aspect Plus 1.76 software (Carl Zeiss, Oberkochen, Germany), with a wavelength range of 560–1690 nm and interval of 3 nm. The integration time was set to 20 ms. RGB (red, green, blue) images were captured with an exposure time of 2.60 ms and were saved in JPEG format with a resolution of 1280 × 960 pixels. Each sample was scanned three times by reloading the other 20 g kernels two times, and the average spectra and images were used.

2.3. Feature extraction and fusion

2.3.1. Spectral features

The original spectra were collected from the middle area of tiled sample in circular shallow tray. Then standard normal variate transformation (SNV) was applied to remove the multiplicative interferences of scatter, particle size, and the change of light distance and reduce environmental effects caused by differences in kernel surface roughness and shape (Wang et al., 2015). Finally, in order to eliminate irrelevant spectral information related to noise and background, two algorithms (competitive adaptive reweighted sampling, CARS, and successive projection algorithm, SPA) were used to extract the characteristic spectral features or bands from the full spectra. In the calculation of CARS, wavelengths with larger absolute regression coefficients of PLSR model are considered as good candidates and selected based on the principle of 'survival of the fittest' from Darwin's Evolution Theory (Li et al., 2009). SPA selects variables with minimal redundancy to solve collinearity problems (Araújo et al., 2001).

2.3.2. Colour features

As for image information, in order to separate wheat grains from background and shallow tray, image threshold segmentation was carried out. Figure 2 shows the RGB (red, green, blue) images of wheat grain samples before and after image segmentation respectively, and the corresponding gray image. Among them, the RGB image of region of interest (ROI) was used to extract six colour features ($\overline{R}$, $\overline{G}$, $\overline{B}$, δ_R, δ_G, δ_B) which represent their mean and variance in RGB mode. Then the RGB tricolour was transformed into HSI (hue, saturation, intensity) mode and additional six feature variables ($\overline{H}$, $\overline{S}$, $\overline{I}$,δ_H, δ_S, δ_I) were extracted from HSI images (Ma et al., 2014). The gray image was used to extract texture features by using gray-level co-occurrence matrix (GLCM) method (Fan et al., 2016; Kekre et al., 2010).

2.3.3. Texture features

GLCM is the statistical method of examining textures that considers the spatial relationship of the pixels, and characterises the texture of an image by calculating how often pairs of pixels with specific values and in a specified spatial relationship occur in an image. A GLCM matrix is a square matrix of size N × N (N is the number of grey levels) with elements corresponding to the relative frequency ($G(i,j)$) of occurrence of pairs of grey level of pixels separated by a certain distance in a given direction. Based on the GLCM, four statistical parameters could be extracted by the following equations: the energy (angular second moment, *ASM*) measures textural uniformity (i.e. pixel pair repetitions):

$$ASM = \sum_{i=1}^{k}\sum_{j=1}^{k}(G(i,j))^2 \quad (1)$$

The entropy (*ENT*) reflects the disorder of the image. For texturally uniform image, entropy is small:

$$ENT = -\sum_{i=1}^{k}\sum_{j=1}^{k}G(i,j)logG(i,j) \quad (2)$$

The contrast (CON) indicates the variance of the gray level:

$$CON = \sum_{i=1}^{k}\sum_{j=1}^{k}(i-j)^2G(i,j) \quad (3)$$

and correlation (COR) measures the similarity of GLCM elements in row or column direction, which reflects the correlation in the local gray image:

$$COR = \sum_{i=1}^{k}\sum_{j=1}^{k}\frac{(ij)G(i,j) - u_i u_j}{s_i s_j} \quad (4)$$

where:

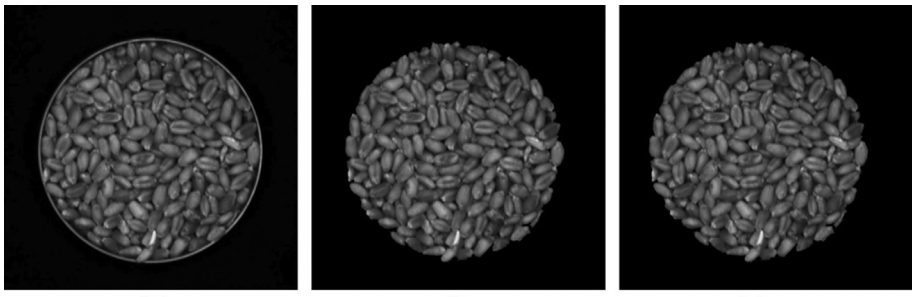

Fig. 2 – RGB images of wheat grains sample (a) before and (b) after image segmentation, (c) the corresponding gray image.

$$u_i = \sum_{i=1}^{k}\sum_{j=1}^{k} i \cdot G(i,j) \quad (5)$$

$$u_j = \sum_{i=1}^{k}\sum_{j=1}^{k} j \cdot G(i,j) \quad (6)$$

$$s_i^2 = \sum_{i=1}^{k}\sum_{j=1}^{k} G(i,j)(i-u_i)^2 \quad (7)$$

$$s_j^2 = \sum_{i=1}^{k}\sum_{j=1}^{k} G(i,j)(j-u_j)^2 \quad (8)$$

Finally, a feature vector is computed using the means and variances of all the four parameters.

2.3.4. Feature fusion

The extracted spectra and 6 colour and 8 texture features were integrated into a data matrix for further analysis to avoid potential information loss and improve reliability. A normalisation procedure was applied to rescale the differences in spectral and colour features before analysis. Then multivariable data analysis was performed to compare the prediction effect of different feature fusion modes. The automatic image segmentation and the feature extraction were conducted in Matlab software (The Mathworks, Natick, USA).

2.4. Multivariable data analysis method

2.4.1. PCA

PCA, as an exploratory unsupervised learning method, is widely used to analyse the data trend and visualise the data distribution. Besides, principal component (PC) spectral analysis is also implemented for selection of key wavelengths. The wavelengths that presented high absolute value of coefficient in the corresponding PC spectra play an important role in modelling analysis (Chu et al., 2017). In this study, PCA was used to analyse the clustering trend of normal (DON $<$ 1 mg kg^{-1}) and contaminated (DON $\geq$ 1 mg kg^{-1}) samples, and the first 10 PCs were used to establish linear discriminant analysis (LDA) models.

2.4.2. Discriminant analysis

Before modelling, the data were divided into a calibration set (2/3 of the total 243 samples) and a prediction set (1/3 of the total 243 samples) by using the Kennard-Stone (KS) method (Said & Mouazen, 2018). Then the LDA, partial least squares discrimination analysis (PLS-DA) and support vector machine (SVM) were used to discriminate wheat grains into normal and DON contaminated categories.

LDA is mainly applied for classification or dimensionality reduction of data, which is useful where the within-class frequencies are inconsistent and random validation data are applied (Ye et al., 2004). As a multivariate statistical method, PLS-DA can integrate the information of independent variables, eliminate the overlapping parts of information, and make the analysis more accurate and reliable (Tang et al., 2014). SVM, as a supervised learning method, can perform the largest discriminant interval between two classes of samples by creating a hyperplane (Teye et al., 2013). All models were evaluated by the correct classification rate (*CCR*), false positive rate (*FPR*) and false negative rate (*FNR*) for calibration and validation sets. *CCR* indicates the percentage of the total number of samples that are correctly predicted. False negative means the DON contaminated samples was misjudged as normal, which is more harmful and should be avoided. So good model should have lower *FPR*, *FNR*, especially *FNR*, and higher accuracy.

2.5. Microstructural analysis

The microstructural changes of acceptable and infected samples with three different DON levels (0.059, 1.148 and 6.233 mg kg-1) were observed using a scanning electron microscope (SEM, Quanta-200, Netherlands). The magnification was set as 2000, and the samples were prepared in flour.

3. Results and discussion

3.1. Spectra and image analysis

The original and SNV pre-treated spectra of all samples (Fig. 3 (a) and (b)) show that the profile of spectral curve of 243 wheat samples is almost the same in the wavelength range of 560–1690 nm. Main absorption peaks were found located at 980 nm, 1225 nm and 1480 nm. The absorption peak at 980 nm mainly related to third overtone of O–H functional group in water and starch, and the absorption peak at around 1225 nm was due to the third overtone of C–H in protein and starch, and the perceptible peak at 1480 nm appeared because of the second overtone of O–H functional group in glucose. To get a good review of the variation trend of the Vis-NIR spectra of wheat grains with different DON levels, the mean spectra of normal and DON contaminated samples are plotted in Fig. 3 (c). The results show the overlapped spectral curve in the range of 922–1690 nm, and it was noticed that the higher the DON content, the greater the reflectance value in the range of 560–922 nm. The possible reason was that the increase in DON contents might disrupt the cell walls of wheat and amylose, giving the seed coat a pore-like structure and forming a cavity in the aleurone layer, which could lead to an increase in reflectance value (Jin et al., 2014). However, the difference is not obvious, which indicates that is not enough to distinguish the DON contaminated samples from normal ones by spectral information alone.

Figure 4 showed the raw images and corresponding RGB histograms of three different DON contaminated wheat samples (0.234, 2.242 and 4.218 mg kg^{-1}). There was only a subtle difference in RGB images and histograms of three samples, especially for 0.234 mg kg^{-1} and 4.218 mg kg^{-1} samples, which indicates that it is also inadequate to distinguish two categories of samples by only colour features.

The range of mean values and standard deviations (*SD*) for four texture parameters (*ASM*, *ENT*, *CON*, *COR*) are summarised in Table 3. A large overlap of each range existed for the two categories of samples, and there was no significant difference ($p > 0.05$). It can be concluded that effective

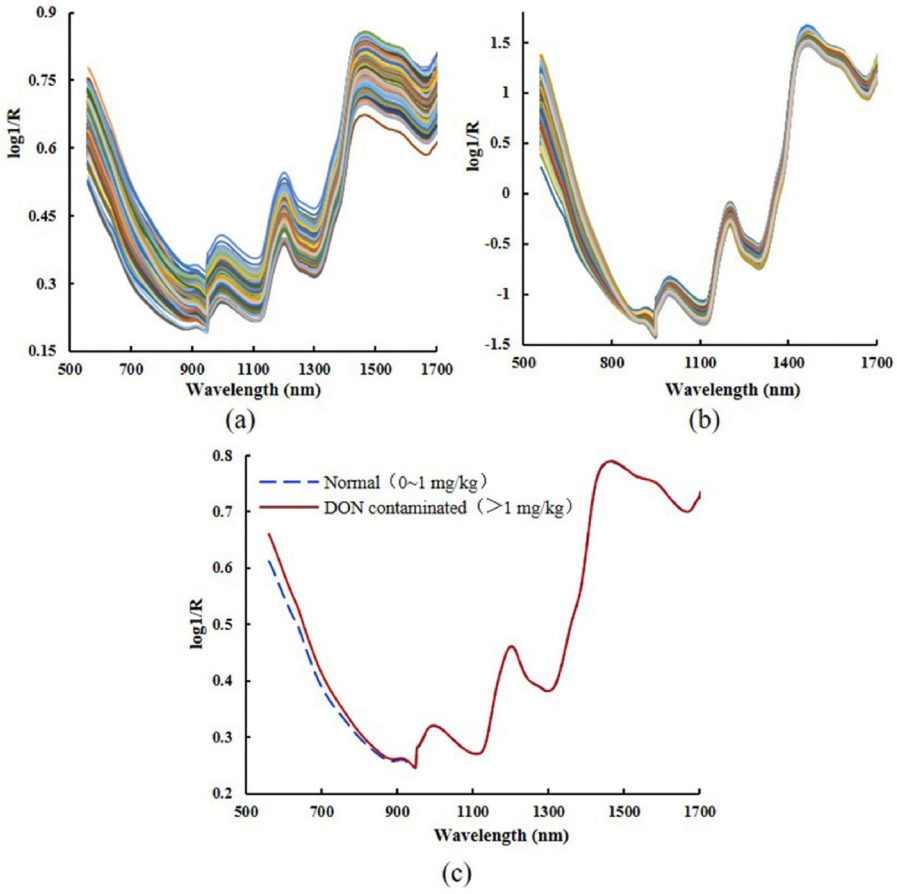

Fig. 3 – Spectral curves of wheat samples with different DON contamination: (a) original spectra (b) SNV pre-treated spectra and (c) average spectra of normal and DON contaminated samples.

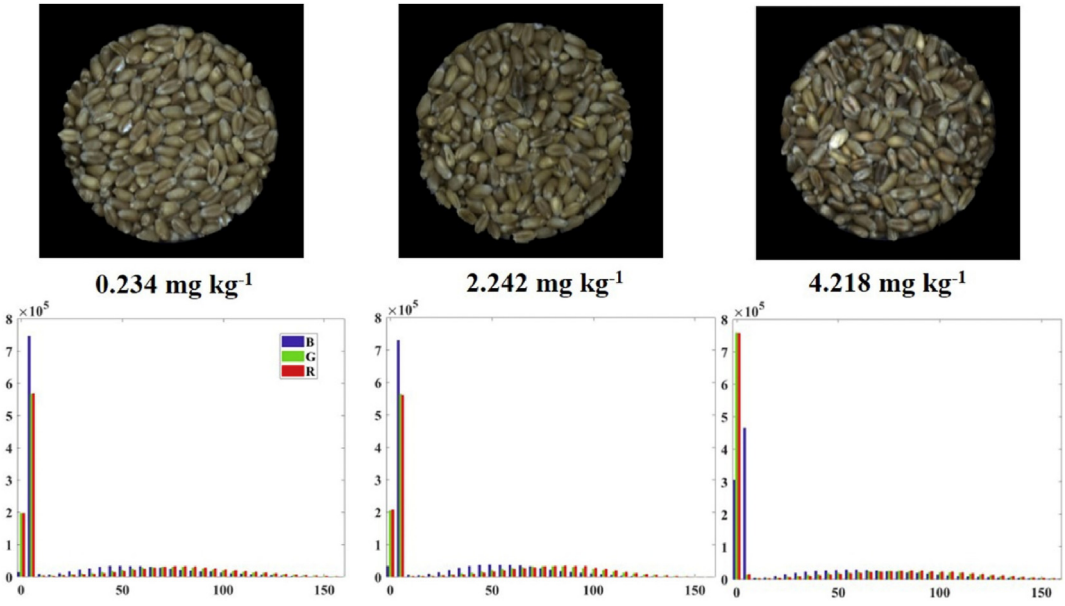

Fig. 4 – Raw images and corresponding RGB histograms of three different DON contaminated (0.234, 2.242 and 4.218 mg kg^{-1}) wheat samples.

classification can hardly be realised by just spectral or image information: feature fusion and further chemometrics analysis was needed to improve the discriminant performance.

3.2. PCA results

All SNV and CARS pre-treated spectra of 243 wheat samples were used for PCA to reveal any possible groupings of the samples according to DON infection level. Figure 5 showed the PC score plot of PC1 and PC2 based on the different combinations of spectral features selected by CARS and colour, texture features. From (a), it can be observed the clustering trend between normal and DON contaminated wheats based on spectral features was not obvious, with many overlapped samples. However, from (b), (c) and (d), the PCs score plot based on image and spectral fusion features obtained a better discrimination than pure spectra, although some samples still overlapped. The overlapping may be due to the DON content in these samples approaching the 1 mg kg^{-1} threshold. The other reason might be related to the fact that only some key information about the basic variable structure concerning a potential possibility of separation of control and contaminated samples was presented by PCA (Kimuli et al., 2018). What is more, these PCs altogether accounted for only less than 70.0% (Fig. 5 (d)) of selected variations, and thus less information of variable structure was reflected in the two dimensional score plots. As DON infection might cause changes in colour and texture of samples, the combination of spectral and image information could reflect more information about different DON concentrations. Overall, PCA was able to roughly distinguish DON contaminated wheat from normal ones, and therefore the supervised discriminant analysis approach was applied further to pursue an improved separation effect.

3.3. Discriminant results

Three classification methods (LDA, PLS-DA and SVM) were applied to sharpen the separation and classify samples into two groups based on spectral and fusion features. The spectral features were optimally selected by using CARS and SPA algorithms respectively, and the number of selected wavelengths, *CCR* for calibration and validation sets for different modelling methods and based on different features are summarised in Table 4. Similar *CCR* were obtained by LDA and PLS-DA methods, and the performance of SVM was the worst. Comparing *CCR* based on two spectra optimisation algorithms, it can be seen that CARS performed better than SPA, perhaps because SPA extracted fewer characteristic wavelengths, resulting in the loss of relevant useful information. By comparing all modelling results, it can be concluded that the LDA model based on spectra (optimised by CARS) and integrated with texture features could realise the best discrimination, with the *CCR* of 95.06% and 91.36% for calibration and validation sets respectively, and the *FNR* of 3.41% and 10.42%, for calibration and validation sets respectively, was the lowest. However, the combination of spectral and colour features could not improve the modelling results. The wheat sample used in DON measurement was not the same as the sample used in image and spectra data acquisition, which may led to misclassification, because the DON distribution is uneven throughout the sample. In future studies, using the same sample for image and spectra acquisition and chemical analysis should be considered.

3.4. Microstructural changes

Microstructural differences between acceptable and infected samples for three different DON levels (0.059, 1.148 and 6.233 mg kg^{-1}) were observed (Fig. 6) using a scanning electron microscope. It could be seen that there were many large and small starch granules inside the normal sample, and the alignment was very close. However, at higher DON content, the binding of starch granules was looser. DON caused by *Fusarium* could enter into starch and protein, resulting in loosening of the bond between starch and protein, which in turn could lead to a decrease in the content of crude starch and crude protein (Wegulo, 2012). These differences suggest that the DON contamination could cause microstructural changes in wheat grains, which would relate to the texture features.

3.5. Discussion

In theory, the detection limit for both Vis-NIR and computer vision techniques cannot reach ppm level because the spectral probe is not sensitive enough (Barbedo et al., 2018). However, as early as 1999, the use of NIR spectroscopy to detect the degree of DON infection in wheat has been reported (Dowell et al., 1999). NIR spectroscopy is an indirect but effective method based on the fact that accumulation of DON results in corresponding changes in NIR–sensitive materials, such as moisture, protein, or more likely colourants. In addition, *Fusarium* infection could not only produce DON, but also change the appearance of wheat kernels (Ruan et al., 2002). Although there have been several studies for detection of

Table 3 – Texture feature statistics.

Texture parameters	Category of samples	Range of mean values	Range of *SD*
ASM	Normal	0.403–0.412	0.086–0.131
	DON contaminated	0.405–0.416	0.091–0.127
ENT	Normal	0.00139–0.00191	0.0201–0.0320
	DON contaminated	0.00140–0.00185	0.0217–0.0323
CON	Normal	1.587–1.838	0.083–0.216
	DON contaminated	1.627–1.799	0.093–0.199
COR	Normal	0.037025–0.044332	0.000135–0.000635
	DON contaminated	0.037979–0.045323	0.000159–0.000530

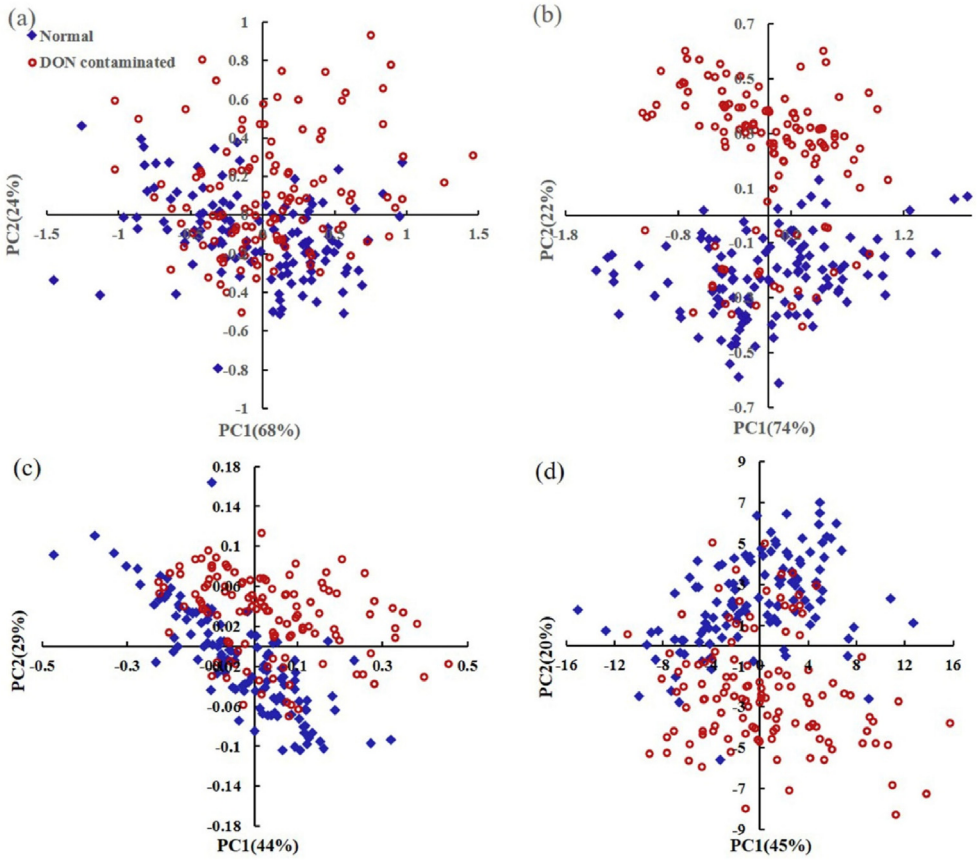

Fig. 5 – Principal component score plots of wheat grains infected with DON: (a) CARS-spectrum, (b) CARS-spectral + colour, (c) CARS-spectral + texture and (d) CARS-spectral + texture + colour. (For interpretation of the references to colour in this figure legend, the reader is referred to the Web version of this article.)

Table 4 – Discriminant results of DON contamination in wheat grains with different integrations of spectra and image features and with different modelling methods.

Modelling method	Features used in modelling	Number of selected wavelengths	Calibration set			Validation set		
		CARS/SPA	CCR (%)	FNR (%)	FPR (%)	CCR (%)	FNR (%)	FPR (%)
			CARS/SPA			CARS/SPA		
LDA	spectra	36/15	88.89/89.51	15.38/11/39	7.14/9.64	86.42/85.19	18.18/16.28	8.11/13.16
	spectra + colour	48/27	95.06/91.36	7.79/14/29	2.25/3.53	85.19/88.89	24.44/17.78	2.78/2.78
	spectra + texture	44/16	95.06/93.21	6.76/11.84	3.41/2.33	91.36/86.42	10.42/21.74	6.06/2.86
	spectra + colour + texture	56/23	91.98/95.06	10.53/10.39	5.81/0	81.48/86.42	25.53/24.44	8.33/0
PLS-DA	Spectra	36/15	88.89/87.04	14.10/13/92	8.33/12.05	88.89/85.19	13.64/18.60	8.11/10.53
	spectra + colour	48/27	95.06/92.59	9.09/14.29	1.18/1.18	85.19/87.65	24.44/17.78	2.78/5.56
	spectra + texture	44/16	93.83/92.59	10.81/11.84	2.27/3.49	87.65/86.42	18.75/21.74	3.03/2.86
	spectra + colour + texture	56/23	92.59/94.44	10.39/10.39	4.71/1.18	82.72/85.19	17.78/24.44	16.67/2.78
SVM	Spectra	36/15	85.19/91.36	16.67/12.66	13.10/4.82	86.42/85.19	18.18/16.28	8.11/13.16
	spectra + colour	48/27	93.21/90.74	11.69/14.29	2.35/4.71	82.72/88.89	28.89/17.78	2.78/2.78
	spectra + texture	44/16	90.12/87.65	14.86/22.37	5.68/3.49	82.72/83.95	27.08/28.26	3.03/0
	spectra + colour + texture	56/23	91.36/91.36	16.88/16.88	1.18/1.18	81.48/80.25	28.89/33.33	5.56/2.78

Fusarium and mycotoxin contamination in wheat grains using NIR and computer vision techniques, few have investigated detection in normally grown and harvested wheat from the field.

The discriminant results indicated that the LDA model based on spectra (optimised by CARS) integrated with texture features could realise the best discrimination, and the integration of colour features did not improve the modelling results. The observation of microstructural differences between levels of DON contamination could be related to the texture features. However, there was no obvious regularity in colour between the normal and DON contaminated samples, so the

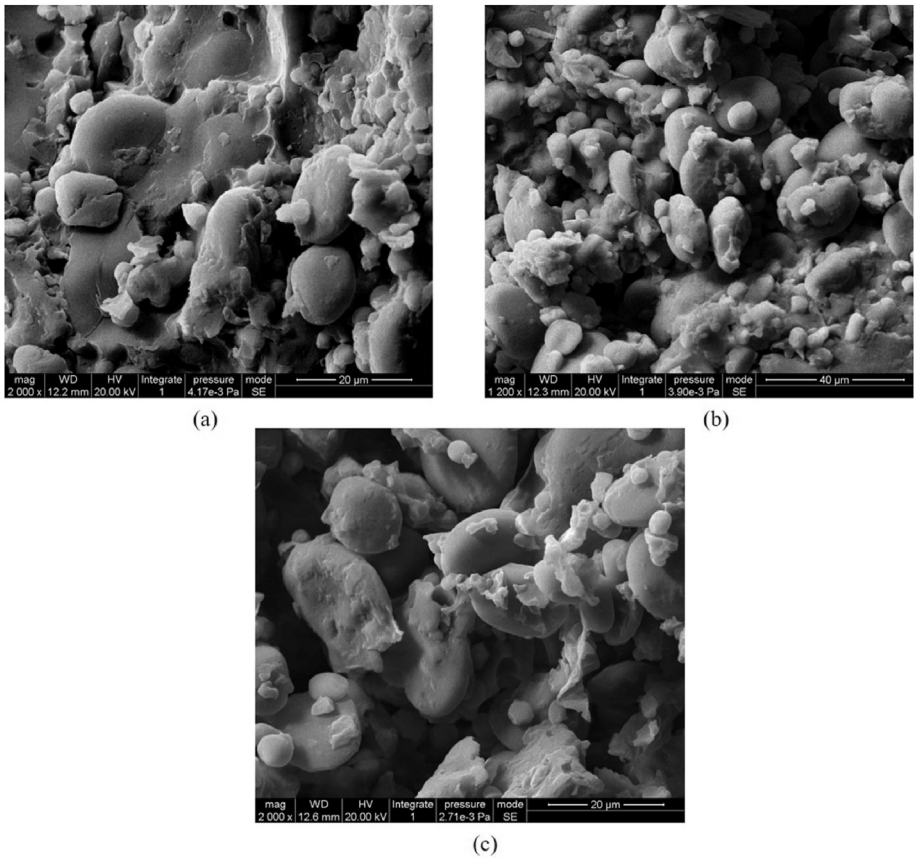

Fig. 6 – Internal scanning results of wheat samples with three different DON levels under 2000-fold magnification electron microscope: (a) 0.059 mg kg^{-1}, (b) 1.148 mg kg^{-1} and (c) 6.233 mg kg^{-1}.

combination of spectral and colour features could not improve the modelling results. For naturally growing wheat with no inoculation and simulated storage, there may be no DON generated when wheat grains were infected by *Fusarium*, but they also appeared mildewed, which may lead to misclassification by using colour features.

4. Conclusions

In this study, Vis-NIR spectroscopy and computer vision techniques were combined to distinguish DON contaminated wheat grains from normal ones. Naturally growing wheat grains collected from various producing areas in China were analysed. In order to verify the advantage of feature fusion, the characteristic spectral variables, colour and texture features were extracted and integrated for chemometric analysis. PCA based on fusion features indicated better clustering tendency than just spectral features. LDA results showed that spectra combined with texture features could achieve the best discrimination with an accuracy of 95.06% and 91.36% for calibration and validation sets respectively, which was 5% higher than just spectral features, and the lowest *FPR*: 3.41% and 10.42% for calibration and validation sets respectively. The internal effects were revealed by SEM pictures. Overall, this research showed that Vis-NIR spectroscopy combined with computer vision has the potential to be used in the non-destructive and online detection of DON contaminated wheat grains. However, the online detection system was laboratory-based with no interference of dust and vibration, so further research will need to be focused on the study of influence of environmental and other factors on the sorting results for actual on-line detection.

Declaration of competing interest

The authors declare that they have no known competing financial interests or personal relationships that could have appeared to influence the work reported in this paper.

Acknowledgements

The authors appreciate the support provided by National Natural Science Foundation of China (No. 31772061), Youth Science Fund of Jiangsu Province (No. SBK2020042843), Postgraduate Research & Practice Innovation Program of Jiangsu Province (No. KYCX19_1419) and the Project Funded by the Priority Academic Program Development of Jiangsu Higher Education Institutions (PAPD).

REFERENCES

Araújo, M. C. U., Saldanha, T. C. B., Galvao, R. K. H., Yoneyama, T., Chame, H. C., & Visani, V. (2001). The successive projections algorithm for variable selection in spectroscopic multicomponent analysis. *Chemometrics and Intelligent Laboratory Systems, 57*, 65–73.

Bai, G., & Shaner, G. (2004). Management and resistance in wheat and barley to Fusarium head blight. *Annual Review of Phytopathology, 42*, 135–161.

Barbedo, J. G. A., Guarienti, E. M., & Tibola, C. S. (2018). Detection of sprout damage in wheat kernels using NIR hyperspectral imaging. *Biosystems Engineering, 175*, 124–132.

Bayraktar, B., Banada, P. P., Jr., Bhunia, A. K., Robinson, J. P., & Rajwa, B. P. (2006). Feature extraction from light-scatter patterns of Listeria colonies for identification and classification. *Journal of Biomedical Optics, 11*, 034006-1-8.

Chen, H., Wang, J., Yuan, Q., & Wan, P. (2011). Quality classification of peanuts based on image processing. *Journal of Food Agriculture and Environment, 9*, 205–209.

Chen, H., Xiong, L., Hu, X., Wang, Q., & Wu, M. (2007). Identification method for moldy peanut kernels based on neural network and image processing. *Transactions of the Chinese Society of Agricultural Engineering, 23*, 158–161.

Chu, X., Wang, W., Yoon, S. C., Ni, X., & Heitschmidt, G. W. (2017). Detection of aflatoxin B1 (AFB1) in individual maize kernels using short wave infrared (SWIR) hyperspectral imaging. *Biosystems Engineering, 157*, 13–23.

Cunha, S. C., & Fernandes, J. O. (2012). Development and validation of a gas chromatography-mass spectrometry method for determination of deoxynivalenol and its metabolites in human urine. *Food and Chemical Toxicology, 50*, 1019–1026.

De Girolamo, A., von Holst, C., Cortese, M., Cervellieri, S., Pascale, M., Longobardi, F., Catucci, L., Porricelli, A. C. R., & Lippolis, V. (2019). Rapid screening of ochratoxin A in wheat by infrared spectroscopy. *Food Chemistry, 282*, 95–100.

Dowell, F. E., Ram, M. S., & Seitz, L. M. (1999). Predicting scab, vomitoxin, and ergosterol in single wheat kernels using near-infrared spectroscopy. *Cereal Chemistry, 76*, 573–576.

Dvoáek, V., Prohasková, A., Chrpová, J., & toková, L. (2012). Near infrared spectroscopy for deoxynivalenol content estimation in intact wheat grain. *Plant Soil and Environment, 58*, 196–203.

Fan, S., Zhang, B., Li, J., Liu, C., Huang, W., & Tian, X. (2016). Prediction of soluble solids content of apple using the combination of spectra and textural features of hyperspectral reflectance imaging data. *Postharvest Biology and Technology, 121*, 51–61.

He, X., Fu, X., & Rao, X. (2018). Model robustness improvement by absorption and reduced scattering spectra in short wave near infrared spectral region. *Biosystems Engineering, 176*, 114–124.

Hossain, M. Z., & Goto, T. (2014). Near- and mid-infrared spectroscopy as efficient tools for detection of fungal and mycotoxin contamination in agricultural commodities. *World Mycotoxin Journal, 7*, 507–515.

Jin, F., Bai, G., Zhang, D., Dong, Y., & Dowell, F. (2014). Fusarium-damaged kernels and deoxynivalenol in Fusarium-infected U.S. winter wheat. *Phytopathology, 104*, 472–478.

Kekre, H. B., Thepade, S. D., Sarode, A. K., & Suryawanshi, V. (2010). Image retrieval using texture features extracted from GLCM, LBG and KPE. *International Journal of Computer Theory and Engineering, 2*, 695–700.

Kimuli, D., Wang, W., Jiang, H., Zhao, X., & Chu, X. (2018). Application of SWIR hyperspectral imaging and chemometrics for identification of aflatoxin B1 contaminated maize kernels. *Infrared Physics & Technology, 89*, 351–362.

Kumar, V., Bagwan, N., Koradia, V., & Padavi, R. (2010). Colour sorting-an effective tool to remove aflatoxin contaminated kernels in groundnut. *Indian Phytopathology, 63*, 449–451.

Li, H., Liang, Y., Xu, Q., & Cao, D. (2009). Key wavelengths screening using competitive adaptive reweighted sampling method for multivariate calibration. *Analytica Chimica Acta, 648*, 77–84.

Li, Y., Shi, W., Shen, J., Zhang, S., Cheng, L., & Wang, Z. (2012). Development of a rapid competitive indirect ELISA procedure for the determination of deoxynivalenol in cereals. *Food and Agricultural Immunology, 23*, 41–49.

Ma, J., Sun, D. W., Qu, J. H., Liu, D., & Zeng, X. A. (2014). Applications of computer vision for assessing quality of agri-food products: A review of recent research advances. *Critical Reviews in Food Science and Nutrition, 56*, 113–127.

Moazami, E. F., & Jinap, S. (2009). Optimisation of the determination of deoxynivalenol in wheat flour by HPLC and a comparison of four clean-up procedures. *Food Additives & Contaminants, 26*, 1290–1297.

Pasquali, D., Blundell, M., Howitt, C. A., & Colgrave, M. L. (2019). Catcher of the rye: Detection of rye, a gluten-containing grain, by LC-MS/MS. *Journal of Proteome Research, 18*, 3394–3403.

Qu, J. H., Liu, D., Cheng, J. H., Sun, D. W., Ma, J., Pu, H., & Zeng, X. A. (2015). Applications of near-infrared spectroscopy in food safety evaluation and control: A review of recent research advances. *Critical Reviews in Food Science and Nutrition, 55*, 1939–1954.

Rocha, D. F. D. L., Oliveira, M. D. S., Furlong, E. B., Junges, A., Paroul, N., Valduga, E., Backes, G. T., Zeni, J., & Cansian, R. L. (2017). Evaluation of the TLC quantification method and occurrence of deoxynivalenol in wheat flour of southern Brazil. *Food Additives & Contaminants Part A Chemical Analysis Control Expo Risk Assess, 34*, 2220–2229.

Ruan, R., Li, Y., Lin, X., & Chen, P. (2002). Non-destructive determination of deoxynivalenol levels in barley using near-infrared spectroscopy. *Applied Engineering in Agriculture, 18*, 549–553.

Said, N., & Mouazen, A. M. (2018). Optimal sample selection for measurement of soil organic carbon using on-line vis-NIR spectroscopy. *Computers and Electronics in Agriculture, 151*, 469–477.

Shen, F., Wu, Q., Liu, P., Jiang, X., & Fang, Y. (2018). Detection of Aspergillus spp. contamination levels in peanuts by near infrared spectroscopy and electronic nose. *Food Control, 93*, 1–8.

Tang, J., Xiang, L., Hong, T., & Jing, G. (2014). GC-MS combined with PLS-DA to discriminate the varieties of Xinjiang lavender essential oil. *Computers & Applied Chemistry, 31*, 701–704.

Teye, E., Huang, X., Dai, H., & Chen, Q. (2013). Rapid differentiation of Ghana cocoa beans by FT-NIR spectroscopy coupled with multivariate classification. *Spectrochimica Acta Part A: Molecular and Biomolecular Spectroscopy, 114*, 183–189.

Walter, S., Nicholson, P., & Doohan, F. M. (2010). Action and reaction of host and pathogen during Fusarium head blight disease. *New Phytologist, 185*, 54–66.

Wang, W., Ni, X., Lawrence, K. C., Yoon, S.-C., Heitschmidt, G. W., & Feldner, P. (2015). Feasibility of detecting Aflatoxin B1 in single maize kernels using hyperspectral imaging. *Journal of Food Engineering, 166*, 182–192.

Wang, Y., Yin, Y., & Zhang, C. (2014). Selective cultivation and rapid detection of Staphylococcus aureus by computer vision. *Journal of Food Science, 79*, M399–M406.

Wegulo, S. N. (2012). Factors influencing deoxynivalenol accumulation in small grain cereals. *Toxins, 4*, 1157–1180.

Wu, Q., Xie, L., & Xu, H. (2018). Determination of toxigenic fungi and aflatoxins in nuts and dried fruits using imaging and spectroscopic techniques. *Food Chemistry, 252*, 228–242.

Ye, J., Janardan, R., & Li, Q. (2004). Two-dimensional linear discriminant analysis. *Neural information processing systems*, 1569–1576.